Estuaries Vol. 8, No. 3, p. 256–269 September 1985

Dispersion of Salt and Suspended Sediment in a Partly Mixed Estuary

R. J. UNCLES
R. C. A. ELLIOTT
S. A. WESTON
Natural Environment Research Council
Institute for Marine Environmental Research
Plymouth PL1 3DH
United Kingdom

ABSTRACT: Observations are presented of the transverse and vertical structure of residual water, salt and sediment transport in the upper reaches of a partly mixed estuary. Measurements were made over spring and neap tidal cycles at three sections. The residual transport for each variable exhibited a characteristic transverse structure. This structure is interpreted in terms of fundamental physical processes. The results are used to estimate the relative importance of transverse shear, vertical shear and tidal pumping to the axial dispersion of salt and sediment.

Introduction

The objectives of this paper are to investigate transverse and vertical structure in the transport of water, salt and suspended sediment in the upper reaches of a strongly tidal, partly mixed estuary. The results are used to estimate the relative importance of transverse shear, vertical shear and tidal pumping to the axial dispersion of salt and sediment.

Observations of the transverse structure of currents and salinity have been made for some other estuaries. Generally, these data have been used to delineate the dispersion properties of the estuary studied (Dyer 1974; Hansen 1965; Hughs and Rattray 1980; Hunkins 1981; Murray and Siripong 1978; Rattray and Dworski 1980). Early results indicated that transverse contributions to the shear dispersion of salt were small in a highly stratified estuary, whereas in partly mixed estuaries the transverse and vertical shear contributions were comparable (Dyer 1974). However, recently it has been shown that estimates of the relative importance of transverse and vertical shear dispersion depend sensitively on the method of analysis, and that the role of vertical shear may have been underestimated in some earlier studies (Rattray and Dworski 1980). Therefore, in this paper, particular attention is given to evaluating these contributions to the transport of salt and sediment. In addition to shear processes, tidal pumping can act as an important transport mechanism for salt and sediment in mesotidal and macrotidal, partly mixed and well mixed estuaries (Allen et al. 1980; Hughs and Rattray 1980; Lewis and Lewis 1983; Uncles and Jordan 1980; Uncles et al. 1985).

Some discussion of these various dispersion mechanisms may be of value. Considering salt transport, the salinity and axial velocity at any point on a cross section may each be represented as the sum of a cross-sectional average and a deviation therefrom. The integral over the section area of the product of the velocity and salinity deviations yields the instantaneous rate of salt transport due to shear dispersion. The velocity and salinity deviations will result from inhomogeneities through the water column and across the width. The shear dispersion associated with spatial variations through the column, and across the width, are known as vertical and transverse shear dispersion,

0160-8347/85/030256-14$01.50/0

respectively. Tidal pumping arises in the following way: water entering the estuary on the flood mixes with fresher water in the upper reaches of the estuary. The mixing may be due to small scale turbulence or breaking internal waves, for example. An amount of this mixed water leaves on the ebb flow. Because the flood and ebb flows are roughly equal (the difference being due to freshwater inputs), and the ebb water is fresher than the flood water, this leads to down-estuary pumping of fresher water or, equivalently, an up-estuary pumping of salt.

The experiments were undertaken in the upper reaches of the Tamar Estuary, which is a partly mixed estuary in the southwest of England (Fig. 1). Tides are semidiurnal with mean neap and spring ranges of 2.2 and 4.7 m, respectively.

Observations and Treatment of Data

Three sections (1, 2 and 3; Fig. 1) were occupied for complete spring and neap tidal cycles. The measurements consisted of vertical profiling of velocity, temperature, salinity and suspended sediment at either four or five positions over a cross section. A seatruck was anchored in the central part of each section. An inflatable dinghy was used to travel between, and take measurements at, temporary moorings laid out over the estuary's width. Some of the stations on a section dried out near low water. Measurements were made at half-hourly intervals from the seatruck and at approximately three-quarter-hourly to hourly intervals from the moorings (when submerged). Background data for sections 1 to 3 are given in Table 1. Up-estuary flows are counted negative. The estimated residual flow due to diurnal inequality over the observed tidal cycle is shown.

The transverse topography at sections 1, 2 and 3 is shown in Fig. 2. High and low water lines for the spring and neap tide surveys are shown. Station positions at each section are marked on the high water spring and neap tide lines for the respective surveys. The mean, axial, depth-averaged current speeds across each section are shown in Fig. 2 for both spring and neap tide observations. These distributions were derived from interpolated data on a rectangular grid of points covering each section

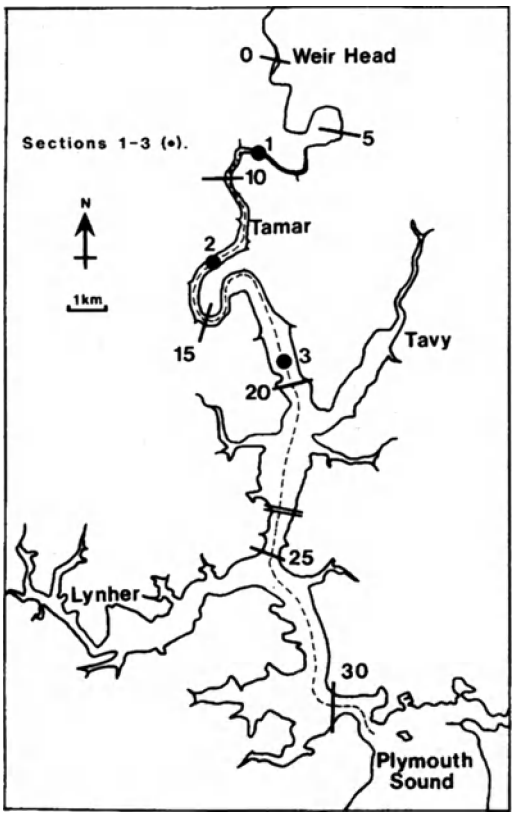

Fig. 1. Sketch chart of the Tamar Estuary showing its subdivision into 5 km intervals and the locations of sections 1 to 3.

(see later). On an intertidal site the mean absolute current speed (over a tidal cycle) was calculated as the average speed during the time for which the site was submerged, times the fraction of the tidal cycle for which this occurred.

In this work, cubic splines were used both to interpolate data at fixed fractions of the depth, and to subsequently define these data at the same instants of time, at all stations over each section, throughout the spring or neap tidal cycle. These instantaneous data were then interpolated onto a rectangular (width, height) grid, with the height directed vertically upwards from the deepest part of the cross section. The chosen interpolation program has been widely used for such problems (Applications Consultants Inc.). An account of the mathematics of the local-fit method of interpolation (used in this work) has been published (Batcha and Reese 1964). The technique was also used to ex-

TABLE 1. Background data for sections 1–3, springs (S) and neaps (N). Residual flows due to daily-averaged run-off, diurnal inequality and their sum, Q, are shown (negative up-estuary).

Section	Date	Tidal Range (m)	Run-off (m^3 per s)	In-equality (m^3 per s)	Q (m^3 per s)
1 (N)	18/5/82	2.3	3.7	−0.5	3.2
2 (N)	19/3/82	1.6	41.8	−1.8	40.0
3 (N)	18/2/82	1.8	21.3	3.8	25.1
1 (S)	25/5/82	4.9	3.6	0.0	3.6
2 (S)	27/4/82	4.6	5.9	0.0	5.9
3 (S)	26/2/82	4.9	25.9	14.3	40.2

trapolate data from the outer stations on each section (Fig. 2) to the banks. Extrapolation is least accurate for the rapidly varying velocity field. In this case, a condition of zero velocity was applied at the bed over the region of extrapolation, and on the banks, so that the problem reverted to one of interpolation.

This procedure was used to generate 12 lunar hourly distributions of axial velocity, U, salinity, S, and suspended sediment, P, over a fixed rectangular grid, for each tidal cycle of data. A summary of the laterally averaged and tidally averaged conditions at sections 1 to 3 is given in Fig. 3. The above technique was used to derive laterally averaged values of velocity, salinity and suspended seidment at fixed fractions of the instantaneous, normalized depth between grid datum and the water surface. Tidal averages were formed from the time-series of these instantaneous profiles: $\langle U_i \rangle$, $\langle S_i \rangle$ and $\langle P_i \rangle$, where the diamond bracket is a tidal average, and where subscript (i) denotes the vertical coordinate (see later).

Considering the tidally averaged salinity, none of these sections could be considered vertically well mixed. Section 2 (Neaps) was strongly stratified, owing to the high run-off (Table 1); this also led to a residual current at section 2 (Neaps) which was directed down-estuary throughout the column. Elsewhere, the residual current showed a classical (although sometimes weak) gravitational circulation.

The tidally averaged concentration of suspended sediment was much higher during spring tides. Maximum values occurred near the bed, which indicates the importance of local resuspension of sediment.

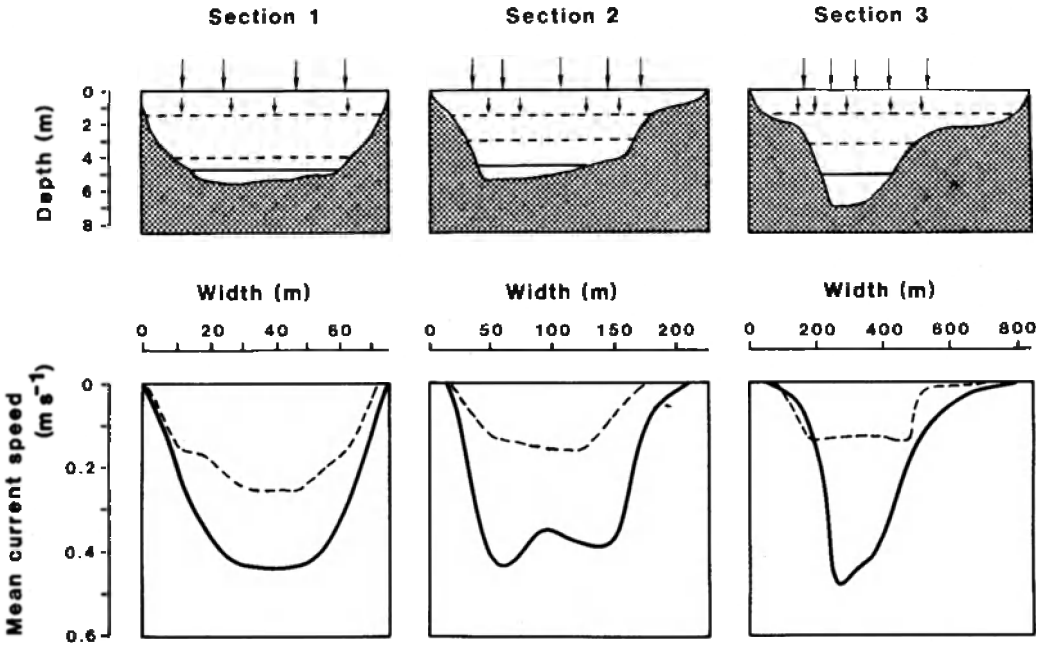

Fig. 2. Topography at sections 1 to 3 and mean tidal current speeds over the width for spring (——) and neap (– – –) observations.

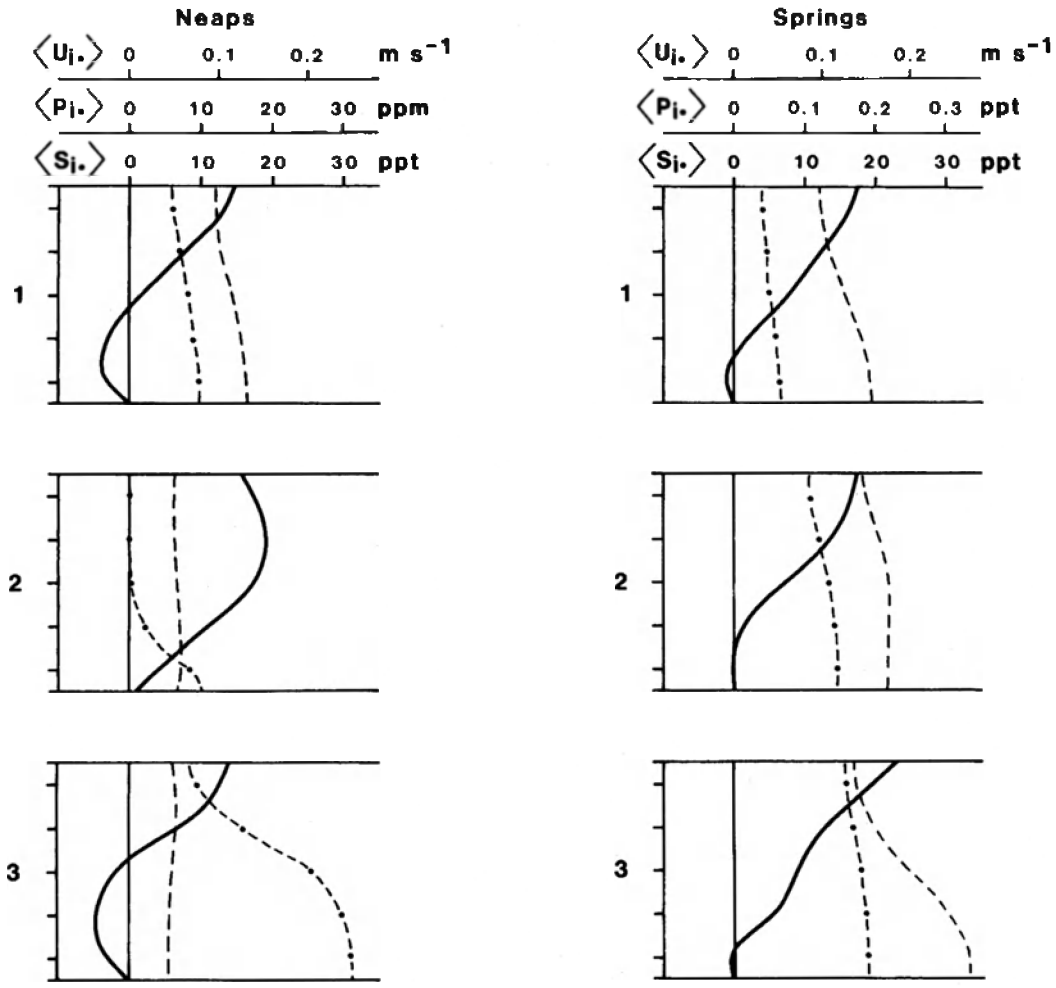

Fig. 3. Vertical profiles of residual velocity (——), sediment concentrations (– – –) and salinity (–·–·–) at sections 1 to 3.

Concentrations during neap tides were small and were typical of levels associated with the freshwater inputs.

Calculation of Transport

The analytical method has been reported previously (Murray and Siripong 1978) and is only briefly outlined here. Values of U, S and P at grid points (i,j) are denoted by U_{ij}, S_{ij} and P_{ij}, where i is row subscript (vertical coordinate), and j is column subscript (transverse coordinate). Each point has a fixed rectangular area, A_{ij}, associated with it, which has the same magnitude for all points. The rates of transport of water, salt and suspended sediment through each element of area are, respectively:

$$Q_{ij} = A_{ij}U_{ij}, \qquad F_{ij} = A_{ij}U_{ij}S_{ij}$$

and

$$G_{ij} = A_{ij}U_{ij}\,P_{ij} \tag{1}$$

Units are m^3 per s for water, ppt m^3 per s (approximately kg per s) for salt, and either ppm m^3 per s (approximately 10^{-3} kg per s) or ppt m^3 per s for suspended sediment.

Transverse means (over the width) are defined at row (i) above grid datum by averaging over water-filled elements A_{ij}. These are denoted by $U_{i.}$ (for velocity). The transverse sum is denoted by U_{it}. Therefore, the

rates of transport through each transverse strip of area centered about row (i) are:

$$Q_{it} = A_{it}U_{i.},\ F_{it} \text{ and } G_{it}$$

Vertical means (over the depth) are defined at column (j) across the width by averaging over rows (i). These are denoted by $U_{.j}$ (for velocity). The vertical sum is denoted by U_{vj}. Therefore, the rates of transport through each vertical strip of area centered about column (j) are:

$$Q_{vj} = A_{vj}U_{.j},\ F_{vj} \text{ and } G_{vj}$$

A cross-sectional average is derived by averaging over all water-filled elements of area A_{ij}. This is denoted by $\bar{U} = U_{..}$ (for velocity). The rates of transport through each section of area $A_{vt} = A$ are given by:

$$Q_{vt},\ F_{vt} \text{ and } G_{vt}$$

Considering the dispersion processes, we define the primary vertical and transverse deviations to be (for velocity):

$$U_{i.}' = U_{i.} - \bar{U} \text{ and } U_{.j}' = U_{.j} - \bar{U}, \quad (2)$$

and the 'interaction' deviation:

$$U_{ij}^* = U_{ij} - (\bar{U} + U_{i.}' + U_{.j}') \quad (3)$$

The rate of transport of salt through a section is given by:

$$F_{vt} = A_{vt}\,\overline{U_{ij}S_{ij}}$$

which, using equations (1)–(3), becomes:

$$F_{vt} = Q_{vt}\bar{S} + A_{vt}\,\overline{U_{i.}'S_{i.}'} + A_{vt}\,\overline{U_{.j}'S_{.j}'} + F_s^* \quad (4)$$

with

$$F_s^* = A_{vt}\overline{U_{i.}'S_{.j}'} + A_{vt}\overline{U_{.j}'S_{i.}'} + A_{vt}\overline{U_{i.}'S_{ij}^*} + A_{vt}\overline{U_{.j}'S_{ij}^*} + A_{vt}\overline{U_{ij}^*S_{i.}'} + A_{vt}\overline{U_{ij}^*S_{.j}'} + A_{vt}\overline{U_{ij}^*S_{ij}^*} \quad (5)$$

We define a tidal oscillation with zero average by a tilde:

$$Q_{vt} = \langle Q_{vt}\rangle + \tilde{Q}_{vt} \text{ and } \bar{S} = \langle \bar{S}\rangle + \tilde{S}$$

The residual rate of transport of salt through a section is:

$$\langle F_{vt}\rangle = \langle F_L\rangle + \langle F_{TP}\rangle + \langle F_{vs}\rangle + \langle F_{st}\rangle + \langle F_s^*\rangle \quad (6)$$

where

$$\langle F_L\rangle = \langle Q_{vt}\rangle\langle \bar{S}\rangle \quad (7)$$

$$\langle F_{TP}\rangle = \langle \tilde{Q}_{vt}\tilde{S}\rangle \quad (8)$$

$$\langle F_{vs}\rangle = \langle A_{vt}\overline{U_{i.}'S_{i.}'}\rangle \quad (9)$$

and

$$\langle F_{st}\rangle = \langle A_{vt}\overline{U_{.j}'S_{.j}'}\rangle \quad (10)$$

In these definitions, $\langle F_L\rangle$ is the rate of transport due to the residual flow of water over the section; $\langle F_{TP}\rangle$ is the rate of transport due to tidal pumping; $\langle F_{vs}\rangle$ is that due to vertical shear dispersion, and $\langle F_{st}\rangle$ that due to transverse shear dispersion. The remaining shear dispersion term is due to interactions between vertical and transverse deviations.

Substituting G for F and P for S in equations (6)–(10) gives an equation for the rate of transport of suspended sediment over a section:

$$\langle G_{vt}\rangle = \langle G_L\rangle + \langle G_{TP}\rangle + \langle G_{vs}\rangle + \langle G_{st}\rangle + \langle G_s^*\rangle \quad (11)$$

The residual rate of transport of water can be written:

$$\langle Q_{vt}\rangle = \langle Q_S\rangle + \langle Q_E\rangle \quad (12)$$

with

$$\langle Q_S\rangle = \langle \tilde{A}_{vt}\tilde{U}\rangle = \langle A_{vt}\rangle\langle \bar{U}_S\rangle \quad (13)$$

and

$$\langle Q_E\rangle = \langle A_{vt}\rangle\langle \bar{U}_E\rangle \quad (14)$$

where $\langle \bar{U}_S\rangle$ is the mass-transport Stokes drift and $\langle \bar{U}_E\rangle$ the sectionally-averaged Eulerian residual current. In addition,

$$\langle Q_{vt}\rangle = \langle A_{vt}\rangle\langle \bar{U}_L\rangle \quad (15)$$

where $\langle \bar{U}_L\rangle$ is the sectionally-averaged, mass transport residual current.

Transport of Water

A summary of the observed residual transport of water is given in Table 2. Symbols are defined in equations (12)–(15). Q is the sum of the daily-averaged freshwater flow across the head of the estuary, and the estimated flow due to diurnal inequality (Table 1). In general, values of Q correspond reasonably well with observed data for the residual volume transport, $\langle Q_{vt}\rangle$. Errors are

TABLE 2. Residual water transport (m^3 per s) and currents (m per s) through sections 1–3 (negative up-estuary).

Section	Q	$\langle Q_{vt} \rangle$	$\langle Q_E \rangle$	$\langle Q_S \rangle$	$\langle \bar{U}_L \rangle$	$\langle \bar{U}_F \rangle$	$\langle \bar{U}_S \rangle$
1 (N)	3.2	3.5 ± 0.5	5.4 ± 0.6	−1.7 ± 0.2	0.023	0.035	−0.011
2 (N)	40.0	41 ± 1	45 ± 1	−3.7 ± 0.3	0.112	0.123	−0.010
3 (N)	25.1	29 ± 3	37 ± 3	−8 ± 1	0.025	0.032	−0.007
1 (S)	3.6	2.3 ± 0.6	12.1 ± 0.7	−9.7 ± 0.4	0.013	0.070	−0.056
2 (S)	5.9	7.5 ± 1.2	33.7 ± 1.7	−26.2 ± 1.1	0.019	0.085	−0.066
3 (S)	40.2	53 ± 6	134 ± 6	−81 ± 2	0.038	0.096	−0.058

95% confidence intervals, and represent minimum values based solely on quoted instrument accuracy (Uncles et al. 1985).

The rate of transport of water due to the mass transport Stokes drift, $\langle Q_S \rangle$, was directed up-estuary at each section. It was much larger during spring tides. This inflow of water arises because of the partially progressive nature of the tide, which, in turn, is a result of frictional dissipation of tidal energy in the estuary (Uncles and Jordan 1980). The head of water produced by this inflow drives a compensating down-estuary flow, $\langle Q_E \rangle$, which satifies $\langle Q_E \rangle = -\langle Q_S \rangle$ in steady-state and in absence of freshwater inputs. The observed rate of transport due to the Eulerian residual current, $\langle Q_E \rangle$, was indeed directed down-estuary (Table 1). $\langle Q_E \rangle$ was comparable with $\langle Q_{vt} \rangle$ during neap tides, but considerably larger during spring tides in order to compensate for the up-estuary flow of water due to the mass transport Stokes drift. Sectionally-averaged residual currents are also shown in Table 2.

Vertical distributions of the residual rate of water transport are shown in Fig. 4. With

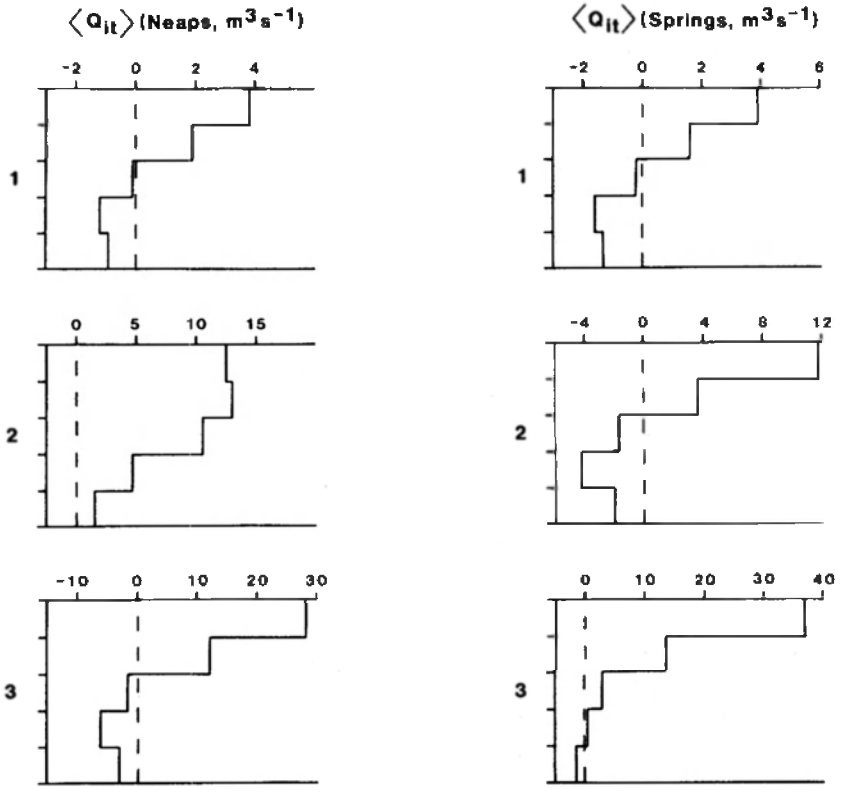

Fig. 4. Vertical profiles of residual transport of water at sections 1 to 3.

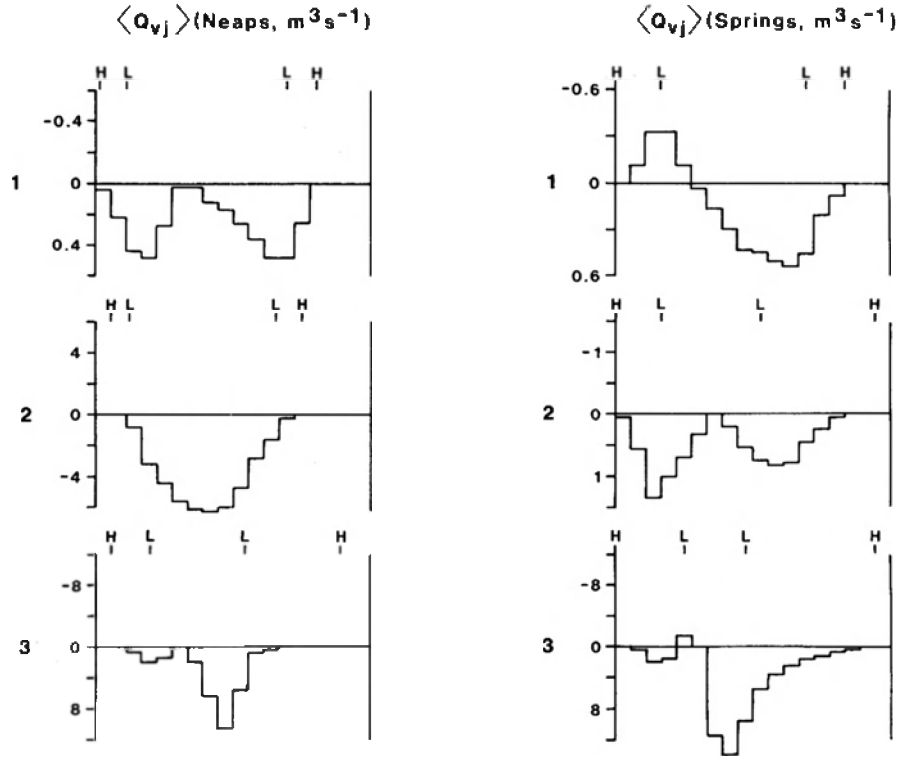

Fig. 5. Transverse distributions of residual transport of water at sections 1 to 3.

the exception of section 2 (Neaps), a classical gravitational circulation of water occurred at each section.

Transverse distributions of the residual rates of water transport, $\langle Q_{vj} \rangle$, at sections 1 to 3 are given in Fig. 5. Values near the high water line (H) are based on extrapolated data (see Fig. 2) and, quantitatively, must be treated with caution. On intertidal areas, between the high (H) and low (L) water lines, the residual rate of transport is defined as the observed average rate of transport during the time the site was submerged times the fraction of time for which this occurred.

At section 2 (Neaps) the distribution showed a simple, river-like form, with fastest speeds in the deeper, central part of the section. Thus, residual currents were mainly caused by the high run-off at that time, and those due to density and tidal effects were secondary. Comparably high run-off also occurred at section 3, but had much less effect there owing to the considerably greater cross-sectional area.

The transverse distribution of residual flow at section 1 (Springs) appeared to be dominated by advective effects. An up-estuary residual flow occurred near the left bank, and a down-estuary flow near the right bank. This was possibly due to centrifugal forcing of the strong spring tidal currents at the bend situated down-estuary of section 1 (Fig. 1).

The remaining distributions showed a systematic pattern of circulation. Flows in the central, deeper part of the section were always very small; they could be directed either up or down-estuary. Over the shallower subtidal and intertidal areas the flow was much stronger and directed down-estuary. This characteristic pattern consisted of three components: (a) a run-off induced residual flow which was directed down-estuary everywhere and had a river-like form; (b) a density-driven component which was down-estuary in the shallow subtidal and intertidal areas and up-estuary in the deeper, central parts of a section; and (c) a tidally-driven component which had a similar form to the density-driven flow. The direc-

TABLE 3. Residual salt transport (ppt m³ per s) through sections 1–3 (negative up-estuary).

Section	$\langle F_{vt} \rangle$	$\langle F_t \rangle$	$\langle F_{TP} \rangle$	$\langle F_s \rangle$	$\langle F_{vs} \rangle$	$\langle F_{st} \rangle$	$\langle F_s^* \rangle$
1 (N)	+13 ± 6	+28 ± 4	+10 ± 3	−25	−24 ± 1	−1	0
2 (N)	+1 ± 5	+54 ± 2	−29 ± 3	−23	−22 ± 4	−5	+4
3 (N)	−14 ± 50	+550 ± 55	−41 ± 11	−526	−460 ± 18	−135	+71
1 (S)	−33 ± 6	+11 ± 3	−24 ± 4	−21	−19 ± 1	0	−2
2 (S)	−34 ± 20	+97 ± 16	−16 ± 14	−115	−111 ± 4	−15	+11
3 (S)	+400 ± 120	+890 ± 120	−290 ± 40	−190	−99 ± 10	−81	−10

tion of residual flow in the center of the channel depended on the combined strength of the density-driven and tidally-induced flows, and the run-off induced flow which opposed them.

Transport of Salt

A summary of the observed residual transport of salt is given in Table 3. Symbols are defined in equations (6)–(10). The residual transport of salt through each section is $\langle F_{vt} \rangle$. Errors are 95% confidence intervals. The sum of the residual transport due to vertical shear, transverse shear and 'interaction' shear is denoted by $\langle F_s \rangle$. Generally, the salt budgets were not in steady-state ($\langle F_{vt} \rangle \neq 0$), as one would anticipate.

The residual rate of transport of salt due to the residual discharge of water was directed down-estuary at all sections. In absence of tidal pumping and shear dispersion, this advective process would have removed saline water from the estuary and replaced it with fresh riverine water. Generally, tidal pumping of salt was directed up-estuary. Thus, tidal pumping was such that fresher water mixed with more saline water (derived from down-estuary) on the flood, and was partially removed on the ebb. At section 1 (Neaps) the tidal pumping per unit width was directed up-estuary in the deeper, central part of the section, but was masked by oppositely directed pumping in the shallower regions.

The residual rate of salt transport due to shear processes over each section, $\langle F_s \rangle$, was directed up-estuary. These processes were therefore diffusive (Fischer et al. 1979). $\langle F_s \rangle$ was either comparable with, or much larger than, the transport due to tidal pumping. This emphasizes the importance of shear dispersive mechanisms even in strongly tidal estuaries. The technique used for estimating errors did not permit their evaluation for $\langle F_s \rangle$, $\langle F_{st} \rangle$ or $\langle F_s^* \rangle$. Of these shear processes, transport due to vertical shear, $\langle F_{vs} \rangle$, was dominant. That due to 'interaction' processes, $\langle F_s^* \rangle$, was very small. Transport due to transverse shear, $\langle F_{st} \rangle$, was also very small except at the widest section, section 3. Here, it was 30% of the vertical shear during the neap tide, and comparable with vertical shear during the spring tide. Thus, as one might expect, transverse shear dispersion becomes more important with increasing width.

The vertical distributions of the total residual rate of salt transport, and that due to vertical shear, are shown in Fig. 6. The vertical distribution of the total residual rate of salt transport is denoted by $\langle F_{it} \rangle$; it showed a similar form to the residual transport of water (Fig. 4). Up-estuary transport of salt in the lower part of the column and down-estuary transport in the near-surface layers were common features at all sections. The up-estuary transport in the lower part of the water column was more pronounced than that for water movements because of the up-estuary transport due to shear dispersion and tidal pumping. The vertical distribution of the contributions to the residual rate of salt transport due to vertical shear is denoted by $\langle (F_{vs})_{it} \rangle$. At each instant, $(F_{vs})_{it}$ is defined by analogy with equation (9) as the sum over columns (j) of $A_{ij}\, U_i'\, S_i'$. Profiles of $\langle (F_{vs})_{it} \rangle$ demonstrate that contributions to the vertical shear dispersion were directed up-estuary throughout the column. These were largest in the near-bed and near-surface layers where the velocity shear and salinity gradient maximized, respectively.

Transverse distributions of the total residual rates of salt transport and that due to transverse shear are shown in Fig. 7. The total residual rate of transport of salt had a characteristic structure over the width which was the same at each section. The salt trans-

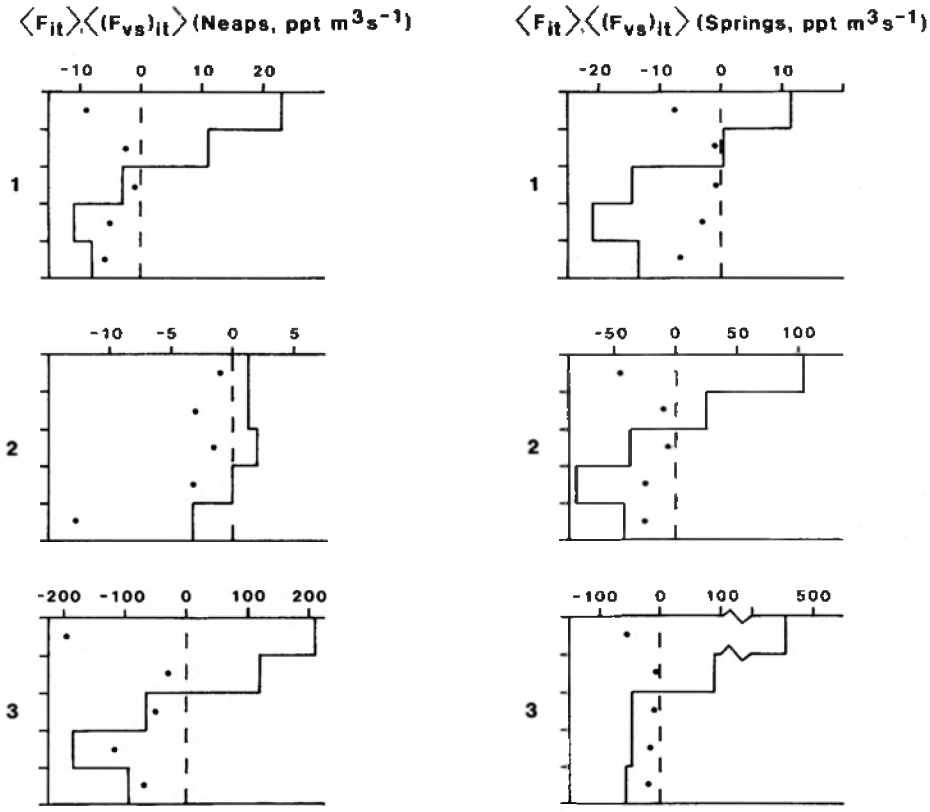

Fig. 6. Vertical profiles of total (——) and shear (●) residual transport of salt at sections 1 to 3.

port was directed up-estuary in the deeper, central part of each section, and down-estuary over shallow and intertidal areas. Because of the minor role of transverse shear dispersion, the observed characteristic pattern consisted essentially of three components per unit width due to: (a) residual water flow; (b) tidal pumping and; (c) vertical shear.

Transverse variations in salinity over a section were small compared with the seasonally-averaged value. Therefore, salt transport due to residual water flow tended to follow the pattern for residual water transport (Fig. 5). For water, this was large and directed down-estuary in the shallow and intertidal areas, and small and directed either up or down-estuary in the deeper part of the section. The salt transport per unit width due to vertical shear was directed up-estuary over the width (not shown) and had maximum values in the deeper parts of the section. Values were negligible over intertidal areas because of the near homogeneity of the shallow water column. Similarly, salt transport due to tidal pumping per unit width (not shown) was directed up-estuary in the deeper parts of a section, where it was largest; it was very small over intertidal areas, where down-estuary pumping sometimes occurred. Thus, the sum of up-estuary-directed tidal pumping and vertical shear dominated the salt transport in the deeper parts of each section, whereas the residual salt transport due to down-estuary-directed residual water discharges dominated in the shallow and intertidal areas.

Contributions to the residual transport due to transverse shear dispersion are shown in Fig. 7. Generally, these were directed up-estuary in the deeper parts of each section. At section 3 the contributions were directed up-estuary over most of the width. The strongest ebb currents on the section tended to be associated with the lowest salinity water; the reverse being the case (although

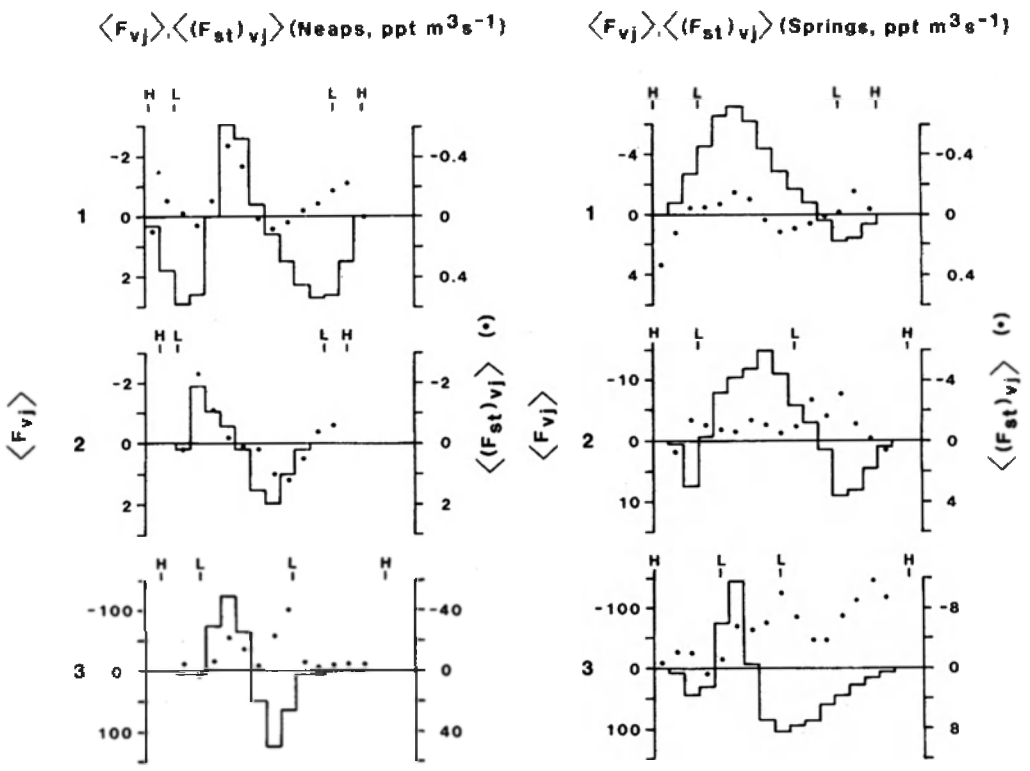

Fig. 7. Transverse distributions of total (——) and shear (●) residual transport of salt at sections 1 to 3.

less pronounced) for the strongest flood currents. These effects generated transverse oscillatory shear dispersion (Fischer et al. 1979; Uncles et al. 1983).

Transport of Suspended Sediment

A summary of the observed residual transport of suspended sediment is given in Table 4. Symbols are defined in equation (11) and have the same meanings as those for the residual salt transport, with G replacing F and P replacing S. The sum of the residual transport due to vertical shear, transverse shear and 'interaction' shear is denoted by $\langle G_s \rangle$.

Residual transport during spring tides was

TABLE 4. Residual sediment transport (ppt m³ per s) through sections 1–3 (negative up-estuary).

Section	$\langle G_w \rangle$	$\langle G_L \rangle$	$\langle G_{TP} \rangle$	$\langle G_v \rangle$	$\langle G_w \rangle$	$\langle G_u \rangle$	$\langle G_s^* \rangle$
1 (N)	−0.03	+0.05	−0.08	0	0	0	0
	(±0.01)	(±0.01)	(±0.01)	—	—	—	—
2 (N)	+0.23	+0.27	−0.01	−0.03	0	−0.03	0
	(±0.01)	(±0.01)	(±0.01)	—	—	—	—
3 (N)	+0.18	+0.17	+0.04	−0.04	+0.02	−0.04	−0.02
	(±0.02)	(±0.02)	(±0.01)	—	—	—	—
1 (S)	−4.0	+0.4	−4.5	+0.08	−0.05	+0.08	+0.05
	(±0.1)	(±0.1)	(±0.1)	—	(±0.04)	—	—
2 (S)	−1.4	+1.6	−2.8	−0.18	−0.24	−0.07	+0.13
	(±0.1)	(±0.3)	(±0.4)	—	(±0.06)	—	—
3 (S)	+24	+12	+12	+0.6	−1.8	+1.0	+1.4
	(±2)	(±1)	(±2)	—	(±0.5)	—	—

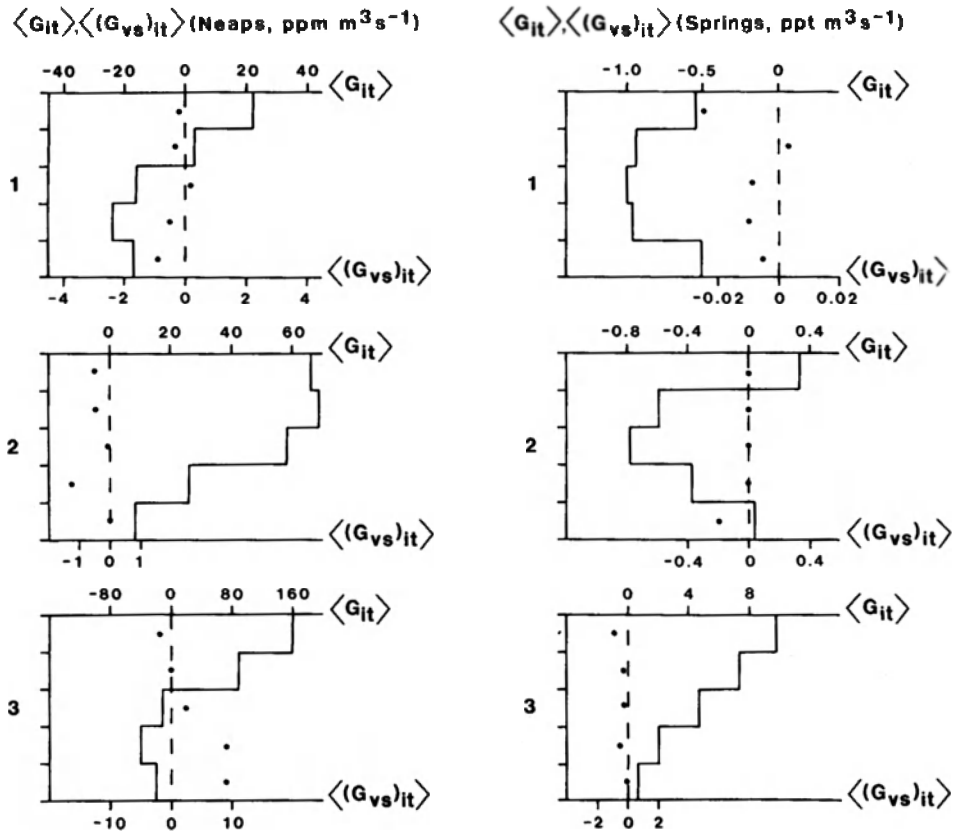

Fig. 8. Vertical profiles of total (——) and shear (●) residual transport of sediment at sections 1 to 3.

between one and two orders of magnitude larger than during neap tides because of the much higher concentrations caused by resuspension of sediment. The residual rate of transport of sediment due to the residual discharge of water was directed down-estuary at all sections. Tidal pumping dominated the transport at spring tides. This pumping of sediment was directed up-estuary at sections 1 and 2, and down-estuary at section 3. Residual rates of transport due to shear processes were very small. During spring tides shear processes were insignificant compared with tidal pumping.

Vertical distributions of the total residual rate of sediment transport $\langle G_{it} \rangle$, and vertical shear $\langle (G_{vs})_{it} \rangle$, are shown in Fig. 8. The residual rate of transport during neap tides closely followed the residual transport of water (Fig. 4). The deep, up-estuary transport at section 1 (Neaps) was enhanced by tidal pumping. Vertical profiles of total residual transport during spring tides were greatly influenced by tidal pumping. At section 1 (Springs) the transport was directed up-estuary throughout the column, with largest values near mid-depth. Most of the resuspension of sediment occurred during the stronger flood tidal currents. Vertical mixing carried this sediment upwards into the faster currents near mid-depth, where large up-estuary transport occurred. Residual transport was less near the surface because of lower concentrations of sediment (due to incomplete mixing from below) and because of the down-estuary transport due to gravitational circulation.

Tidal pumping of sediment was directed up-estuary in the shallow areas of section 2 (Springs); however, it was weak and directed down-estuary in the deeper areas. This, coupled with the down-estuary, near-surface gravitational flow, was sufficient to reverse the direction of residual sediment transport

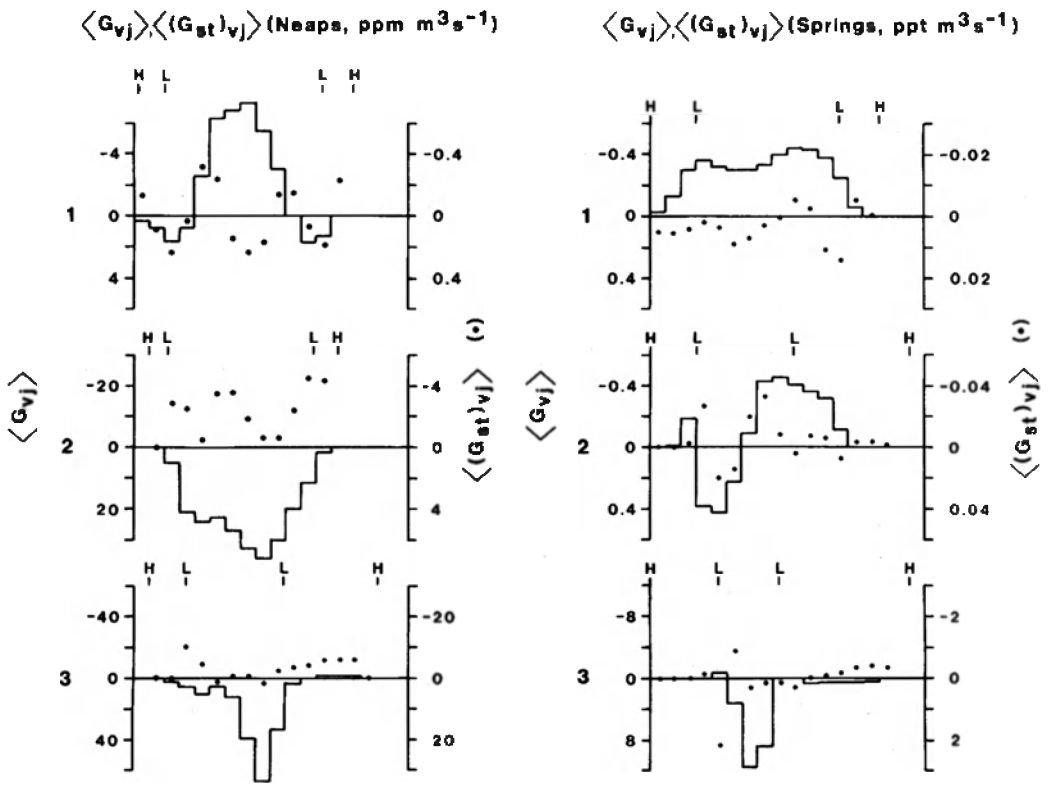

Fig. 9. Transverse distributions of total (——) and shear (●) residual transport of sediment at sections 1 to 3.

in the near-surface and deep layers. At section 3 (Springs) the tidal pumping was strong and directed down-estuary. This generated a vertical profile of residual transport which was directed down-estuary everywhere.

Rates of transport due to vertical shear were very small. With the exception of section 3 (Neaps), contributions to the vertical shear were generally directed up-estuary (Fig. 8). This is consistent with the observation that suspended sediment concentrations increased with depth (as for salinity, Fig. 3). Sediment concentrations decreased with depth at section 3 (Neaps), and contributions to the vertical shear were generally directed down-estuary.

Transverse distributions of the total residual rate of sediment transport and that due to transverse shear are shown in Fig. 9. During neap tides the total rate of transport at sections 2 and 3 closely followed the residual transport of water. At section 1 (Neaps) there was a pronounced up-estuary transport due to tidal pumping—the result of weak resuspension in the flood tidal currents.

The transverse distribution during spring tides was dominated by tidal pumping. The tidal pumping per unit width was directed up-estuary over the whole width at section 1 (not shown) and was much larger than other transport mechanisms. Currents, resuspension, and associated sediment transport were much higher during the flood than during the ebb. Flood currents also exceeded ebb currents at section 2 (Springs), and up-estuary transport due to tidal pumping occurred in the shallow and intertidal areas where sediment was available for resuspension. However, weak, down-estuary pumping in the deep part of the section enforced the residual advective transport, $\langle G_L \rangle$, and produced a strong down-estuary transport of sediment. The down-estuary pumping was due to the absence of easily erodible bed sediment in the deepest part of the section. Because of the up-estuary increase in suspended sediment concentration, pumping

of sediment acted in the opposite way to pumping of salt, and caused a down-estuary transport. This picture was exaggerated at section 3 (Springs). Here, asymmetry between flood and ebb currents was small, and the up-estuary pumping in shallow and intertidal areas was weak. Transport due to transverse shear was very small, and contributions to the shear showed little systematic structure over the width (Fig. 9).

Conclusions

The observations showed that large transverse variations in water, salt and sediment fluxes occurred in the upper reaches of the Tamar Estuary. The total residual rate of transport of water showed a characteristic transverse structure for four of the six tidal cycles. The transport was large and directed down-estuary over the shallow and intertidal areas; in the deeper parts of a section it was small and could be directed up- or down-estuary. This circulation is the transverse analogue of the vertical gravitational circulation.

Transport of salt due to vertical shear was always directed up-estuary. The total residual transport of salt had a characteristic structure over the width. Transport was directed up-estuary in the deeper, central parts of a section, and down-estuary in the shallow areas (where down-estuary advection of salt due to the residual flow of water dominated the transport). Neither tidal pumping nor shear dispersion could be neglected. Vertical shear dispersion dominated that due to transverse shear. This was a consequence of the high correlation between velocity and salinity variations in the vertical, as opposed to the poorer correlation between their transverse variations. Rattray and Dworski (1980) found that this was also the case for Southampton Water. Transverse shear dispersion was very small in the narrow sections near the head (width less than 200 m), but was comparable with the vertical shear dispersion at the widest section (width 800 m) during spring tides.

The fluxes of suspended sediment were dominated by tidal pumping at spring tides. The residual transport of sediment was directed up-estuary over the whole width near the head. This was a consequence of the strong asymmetry of the tidal currents and is thought to have important implications for the formation and magnitude of the turbidity maximum. Maximum current speeds and associated resuspension and sediment transport were much higher during the flood than the ebb. The tidal asymmetry persisted down-estuary but was weaker. Here, the residual transport of sediment was directed down-estuary in the deeper part of a section. This was due to the absence of easily erodible bed sediment. Fine sediment was available for resuspension only in the shallow and intertidal areas where it could be pumped into the estuary. Because the suspended sediment concentration increased towards the head (opposite to salinity), the tidal pumping of sediment in the deep areas (in absence of local resuspension) transported fresher, more turbid water down-estuary (opposite to the pumping of salt). Transport was much smaller at neap tides, but weak resuspension and tidal pumping occurred near the head.

The experimental results for salt transport differ markedly from deductions based on theoretical, steady-state considerations of shear dispersion in the Tamar (Uncles et al. 1983). Using currently employed formulae (Fischer et al. 1979), it was found that vertical shear dispersion was negligible in the upper estuary. Moreover, using an estimated (unmeasured) value for cross-estuary mixing, it was found that dispersion due to transverse oscillatory shear was comparable with observed data. Clearly, considerable doubt exists as to the usefulness of applying these theoretical formulae to strongly tidal, partly mixed estuaries such as the Tamar, where little is known about either vertical or transverse mixing processes.

Although our results apply to the Tamar Estuary, they have wider implications for analytical and numerical modelling studies of partly mixed estuaries in general. The importance of the vertical gravitational circulation and its associated pattern of salt transport has been recognized for many years. Our data show that characteristic, strong circulation patterns for water and salt transport also exist over the width. Such patterns cannot, of course, be resolved with

the two-dimensional (depth-axis) models which have traditionally been deployed to describe partly-mixed estuaries. Nevertheless, because of the dominance of vertical shear dispersion of salt over transverse shear dispersion, it seems likely that the (depth-axis) models could supply reasonable estimates of the shear transport of salt, providing the time-dependent, within-tide turbulent mixing coefficients were known sufficiently accurately. The importance of tidal pumping to the salt transport also indicates that steady-state simulations are, in general, not realistic. Tidal flows and within-tide turbulent mixing must be taken into account in order to simulate this mode of transport.

Our data demonstrate the existence of strong transverse variations in the suspended sediment transport within partly-mixed estuaries. The comparative unimportance of shear processes to the transport indicates that depth-integrated (width-axis) models could supply reasonable estimates of the suspended sediment transport.

Acknowledgments

We are grateful to Mr. J. A. Stephens and Ms. T. Woodrow for assistance with data analyses, illustrations and word-processing. This work forms part of the Physical Processes programme of the Institute for Marine Environmental Research, a component of the Natural Environment Research Council (NERC). It was partly supported by the Department of the Environment on contract No. DGR 480/48.

Literature Cited

Allen, G. P., J. C. Salomon, P. Bassoullet, Y. Du Perihoat, and C. De Grandpre. 1980. Effects of tides on mixing and suspended sediment transport in macrotidal estuaries. *Sediment. Geol.* 26:69–90.

Applications Consultants Inc. Surface approximations and contour mapping (SACM). Houston, Texas, USA.

Batcha, J. P., and J. R. Reese. 1964. Surface determination and automatic contouring for mineral exploration, extraction, and processing. *Q. J. Colorado Sch. Mines* 59:1–14.

Dyer, K. R. 1974. The salt balance in stratified estuaries. *Estuarine Coastal Mar. Sci.* 2:273–281.

Fischer, H. B., E. J. List, R. C. Y. Koh, J. Imberger, and N. H. Brooks. 1979. Mixing in Inland and Coastal Waters. Academic Press, New York. 484 p.

Hansen, D. V. 1965. Currents and mixing in the Columbia River Estuary. Trans. Joint Conf. on Ocean Sci. and Ocean Engineering. p. 943–955.

Hughs, F. W., and M. Rattray. 1980. Salt fluxes and mixing in the Columbia River Estuary. *Estuarine Coastal Mar. Sci.* 10:479–493.

Hunkins, K. 1981. Salt dispersion in the Hudson Estuary. *J. Phys. Oceanogr.* 11:729–738.

Lewis, R. E., and J. O. Lewis. 1983. The principal factors contributing to the flux of salt in a narrow, partially stratified estuary. *Estuarine Coastal Shelf Sci.* 16:599–626.

Murray, S. P., and A. Siripong. 1978. Role of lateral gradients and longitudinal dispersion in the salt balance of a shallow well mixed estuary, p. 113–124. *In* B. Kjerfve (ed.), Estuarine Transport Processes. Univ. South Carolina Press.

Rattray, M., and J. G. Dworski. 1980. Comparison of methods for analysis of the transverse and vertical circulation contributions to the longitudinal advective salt flux in estuaries. *Estuarine Coastal Mar. Sci.* 11:515–536.

Uncles, R. J., and M. B. Jordan. 1980. A one-dimensional representation of residual currents in the Severn Estuary and associated observations. *Estuarine Coastal Mar. Sci.*. 10:39–60.

Uncles, R. J., A. J. Bale, R. J. M. Howland, A. W. Morris, and R. C. A. Elliott. 1983. Salinity of surface water in a partially-mixed estuary, and its dispersion at low run-off. *Oceanol. Acta* 6:289–296.

Uncles, R. J., R. C. A. Elliott, and S. A. Weston. 1985. Observed fluxes of water, salt and suspended sediment in a partly mixed estuary. *Estuarine Coastal Shelf Sci.* 20:147–167.

Received for consideration, October 29, 1984
Accepted for publication, June 19, 1985